Distributed Observer-based Prescribed Performance Control for Multi-Robot Deformable Object Cooperative Teleoperation

Zhenyu Lu, Ning Wang, *Member, IEEE,* Weiyong Si, and Chenguang Yang, *Senior Member, IEEE*

Abstract—**In this paper, a distributed observer-based prescribed performance control method is proposed for using a multi-robot teleoperation system to manipulate a common deformable object. To achieve a stable position-tracking effect and realize the desired cooperative operational performance, we define a new hybrid error matrix to represent the errors of both the relative distances and absolute positions of robots and then decompose the matrix into two new error terms for cooperative and independent robot control. To enable the desired handling of the deformable object by the robots, we improve the Kelvin-Voigt (K-V) contact model based on the new error terms. Because the center position and deformation of the object cannot be directly measured, the object dynamics are then expressed by the relative distances of robots and an equivalent impedance term. Each robot incorporates an observer to estimate contact force and object dynamics based on its own measurements. To address the position errors caused by biases in force estimation and realize the position-tracking effect of each robot, we improve the barrier Lyapunov functions (BLFs) by incorporating the errors into system control. which allows us to achieve a predefined position-tracking effect. We conduct an experiment to verify the proposed controller's ability to balance robustness and position-tracking effectiveness in a dual-telerobot cooperative manipulation task, even when the object is subjected to unknown disturbances.**

Note to Practitioners— **This article is inspired by the limitations of multi-telerobot manipulation with a deformable object, where the deformation of the object cannot be measured directly. Meanwhile, force sensors, especially 6-axis force sensors, are very expensive. To realize the purpose that objects manipulated by multiple robots match the same state as operated on the leader side, we propose an object-centric teleoperation framework based on the estimates of contact forces and object dynamics and the improved barrier Lyapunov functions (BLFs). This framework contributes to two aspects in practice: 1) propose a control diagram for deformable object co-teleoperation of multi-robots for unmeasurable object's centre position and deformation; 2) propose an improved BLFs controller based on the estimation of contact force and robot dynamics. The estimation errors are considered and transferred using an equivalent impedance to be integrated into the Lyapunov function to minimize both force and motion-tracking errors. The experimental results verify the effectiveness of the proposed method. The developed framework can be used in industrial applications with a similar scenario..**

Index Terms— **Cooperative teleoperation, Multi-robot system, Deformable object manipulation, Barrier Lyapunov Functions, Distributed observer**

I. INTRODUCTION

MULTILATERAL telerobots have been widely applicable in surgical operations and flexible and dexterous human-robot interaction [1]-[4]. Compared to single-arm teleoperation robotic systems, two-arm and multi-arm telerobot systems can complete complex tasks with stronger manipulation capacity and higher efficiency [5]-[7].

This paper focuses on a multilateral telerobot system that comprises several manipulators on the leader side and an equal number of robots on the follower side. For this research topic, Sirouspour has proposed a μ synthesis-based control diagram to address the problem of follower robots utilizing a tool for cooperative manipulation of the environment [8]. The research and model were further developed by Chen *et al.* [9], [10], Thanh *et al.* [11] and Azimifar *et al.* [12]. For instance, Chen *et al.* focused on adaptive robust control for multilateral telerobot systems with arbitrary time delays considering the influence of external disturbances, parametric uncertainties, and modeling errors [9], [10]. Thanh *et al.* [11] compared the centralized and decentralized control diagrams for the system and pointed out that the decentralized control mode has higher fault tolerance ability, better flexibility and higher reliability. Azimifar *et al.* discussed system transparency and proposed a force estimator to estimate the external force which can realize the stability and transparency of a closed-loop control [12]. Moreover, the work of Sun *et al.* [13] on cooperative grasping with reconfigurable robots was based on type 2 fuzzy logic control, which was also a special case for multilateral teleoperation systems.

Most of the aforementioned studies heavily rely on precise geometric models of the objects and robots, along with accurate force measurements. However, they overlook the deformation and dynamic changes that occur at the objects and robots due to the cooperative efforts of multiple telerobots. These factors are critical in real-world robot manipulation. Even a slight error in motion can lead to substantial contact forces on a rigid object, resulting in potential damage to both the robots and the object.

This work was partially supported by Engineering and Physical Sciences Research Council (EPSRC) under Grant EP/S001913 and the H2020 Marie Sklodowska-Curie Actions Individual Fellowship under Grant 101030691. (Corresponding author: Chenguang Yang)

The authors are with the Bristol Robotics Laboratory, University of the West of England, BS16 1QY, United Kingdom, (E-mail: luzhenyurobot@gmail.com ; katie.wang@brl.ac.uk; weiyong.si@uwe.ac.uk, cyang@ieee.org).

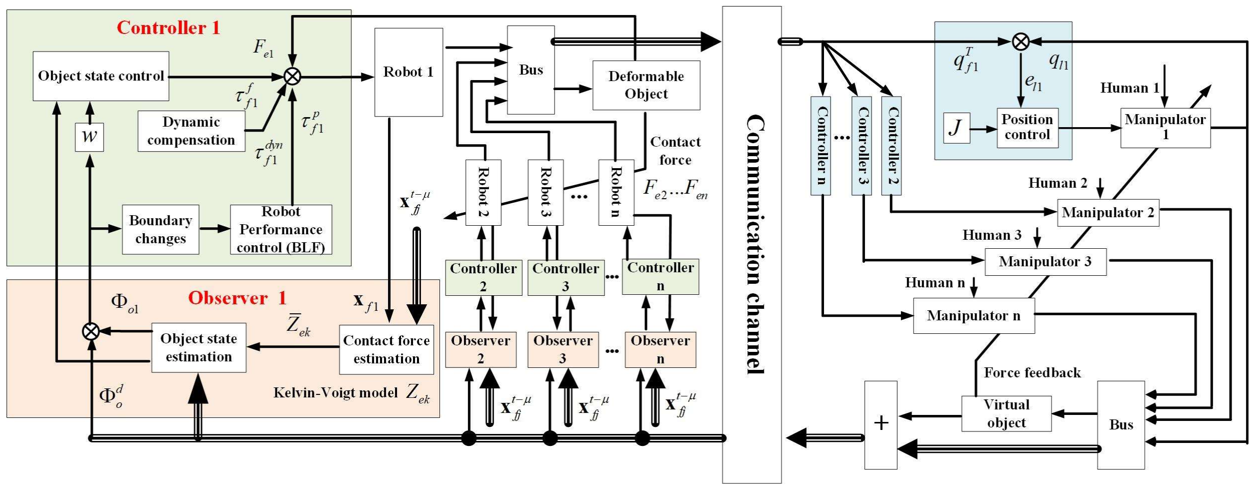

Fig. 1. Draft diagram of the proposed collaborative multi-leader multi-follower teleoperation for a deformable object.

The position tracking performance in teleoperation systems depends on the accurate estimation of contact force. Therefore, some researchers have investigated force-independent control, where neural networks are used to estimate and compensate for force or torque errors [12]-[16], which is especially useful for space operations [17].

In this paper, we will design a new decentralized controller for a multi-robot teleoperation system by creating distributed observers to estimate the contact force of each robot and the dynamics of deformable objects. Compared to the centralized control mode, such as the model-mediated teleoperation [18], the distributed controller can balance the common manipulation effect and self-interaction in a flexible contact task [11]-[12]. Meanwhile, multi-robot teleoperation for a deformable object has not been extensively researched previously. This paper will investigate the oscillations increasing phenomenon caused by unbalanced output forces and varying time delays during the information distribution process as well [19]. This research is based on our previous research on multi-leader multi-follower (MLMF) teleoperation [20]-[23], cooperative manipulation of dual-arm robots [24], [25], and force sensorless control [12]-[16], [26]. The control diagram for the n -manipulator- n -robot teleoperation system is illustrated in Fig.1. The symbols such as τ_{f1}^{f} , F_{e1} *et al.* are introduced in Table 1, Section II. A.

On the follower side, we build several distributed observers to estimate unknown object deformations and dynamics based on the Kelvin-Voigt (K-V) contact model. The outputs of these observers are then used for follower controllers to balance the common operational effect and the self-stability control. The Barrier Lyapunov function (BLF) is also improved and used in the follower controllers to specify the robots' performance. The leader controllers are designed to interact with the operators to handle a virtual object through a force-feedback interface. The key contributions of this paper are shown as follows:

1) We propose teleoperation system stability conditions from the perspectives of object manipulation and robot motion tracking. Using the K-V model, we derive a coupled error matrix and then decompose the matrix into two kinds of error terms for the controller and the observer design. The interactions between the robots and objects are simplified and expressed by measurable variables and an equivalent impedance factor $\bar{Z}_{ek}$.
2) We build a high-gain distributed observer to estimate the contact force and the object dynamics of each robot based on known dynamics parameters, real-time measurements and delayed communications among the robots. A torque term τ_{fk}^{f} in Fig.1 is built based on the estimations that are used to minimize the errors in object-level manipulation.
3) To limit object dynamics estimation errors and realize the predefined control performance, we improve the BLFs and build term τ_{fk}^{p} in Fig.1 for robot control. Unlike nonlinear compensation terms using neural networks (NN) [24], the proposed method does not need pre-training and directly transfer the torque errors to varying boundary conditions, thereby maintaining the system passivity.

The remainder of this paper is organized as follows: Section II shows the teleoperation system model and control objectives. Section III designs the observers and controllers, and Section IV proves system stability. Section V verifies the effectiveness of the proposed method through experiments, while Section VI provides the final conclusion.

II. System Modelling and Control Objective

A. System modelling

Using the symbols in Table 1, we describe the teleoperation system consisting n robots and n manipulators in a Lagrange form as:

$$\begin{cases} M_{lj}\left(q_{lj}\right)\ddot{q}_{lj}+C_{lj}\left(q_{lj},\dot{q}_{lj}\right)\dot{q}_{lj}+G_{lj}=J_{lj}^{T}(q_{lj})F_{hj}-\tau_{lj} \\ M_{fj}\left(q_{fj}\right)\ddot{q}_{fj}+C_{fj}\left(q_{fj},\dot{q}_{fj}\right)\dot{q}_{fj}+G_{fj}=\tau_{fj}-J_{fj}^{T}(q_{fj})F_{ej} \end{cases},(1)$$

where $M_{ij}(q_{ij})$ and $C_{ij}\left(q_{ij},\dot{q}_{ij}\right)$, $i=l,f$, $j=1,...,n$ are the inertia matrix and the centripetal and Coriolis matrix. They are simply expressed as M_{ij} and C_{ij} . G_{ij} is the gravitational torque, and $J_{ij}(q_{ij})$ is the Jacobian matrix, and we have

$$x_{ij}=p\left(q_{ij}\right), \qquad (2)$$
$$\dot{x}_{ij}=\dot{p}\left(q_{ij}\right)=J_{ij}(q_{ij})\dot{q}_{ij}.$$

TABLE 1.
SYMBOLS AND MEANINGS

Symbol	Meanings
$*_{ij}, i = l, f,$ $j, k = 1, \ldots, n$	i represents the leader and follower robots, and j and k represents the number of robots
$*^{d(t)}$	Delayed signal with time delays $d(t)$
q_{ij}, q_{ij}^d	Real and desired robots joints
x_{ij}, x_{ij}^d	Real and desired robot end positions
$\tau_{ij}, \tau_{fj}^f, \tau_{fj}^p, \tau_{fj}^{dyn}$	τ_{ij} is the control torque and other symbols are part of τ_{sj}
η_{ij}	Position tracking errors $\eta_{ij} = x_{ij}^d - x_{ij}$
e_{ij}	Joint tracking errors $e_{ij} = q_{ij}^d - q_{ij}$
F_{hj}	Human force exerting on the manipulator
F_{ej}	Environmental force against the robot ends
x_o	Position of the object center
F_{ext}	External force affected on the object
Φ_o, Φ_o^d	Real and desired values of object dynamics

The object dynamics $\Phi_o(x_o, \dot{x}_o, \ddot{x}_o)$ is expressed as

$$\begin{aligned}\Phi_o(x_o, \dot{x}_o, \ddot{x}_o) &= M_o(x_o)\ddot{x}_o + C_o(x_o, \dot{x}_o)\dot{x}_o + G_o(x_o) \\ &= \sum_{j=1}^{n} J_j F_{ej} + J_e F_{ext}\end{aligned}, \quad (3)$$

where $M_o(x_o)$, $C_o(x_o, \dot{x}_o)$ and $G_o(x_o)$ are the inertia matrix, the centripetal and Coriolis matrix and the gravitational torque of the object, and M_o, C_o and G_o are their simplifications, and J_j and J_e are Jacobian matrices from robots to the object center in the object coordinate. Previous research based on rigid object manipulation assumes that the matrices J_j and J_e are known. However, the method is not applicable to deformable objects since their shape and centre positions change under the effects of multiple robots. Therefore, we propose an equivalent object model in Fig. 2 that represents the deformable object as a hard central object connected with several spring-damping units through the contact points. The deformation of the kth unit is denoted by δ_{fk} and we use the K-V contact model to describe F_{ek} in (3) as

$$F_{ek} = B_e \dot{\delta}_{fk} + K_e \delta_{fk} = Z_e \delta_{fk}, \quad (4)$$

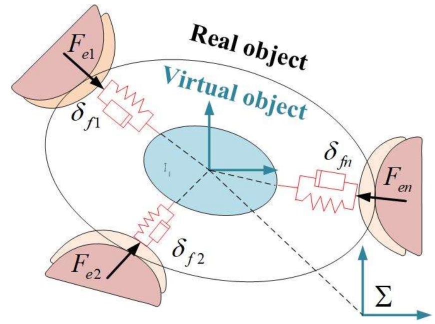

Fig. 2. Illustration of object modelling.

where B_e and K_e are damping and stiffness parameters and $Z_e = B_e s + K_e$ represents the impedance factor for each robot. $\delta_{fk} = \delta_{fk}^o + x_{fk} - x_o$ represents the relative position between the object centre and robots, and $\delta_{fk}^o = \left(x_o - x_{fk}\right)\big|_{t=0^-}$ is the initial position of equilibrium without pressures.

B. Control objective and assumptions

Setting $\tau_{ext} = J_e F_{ext}$ and taking (4) into (3) , we get

$$\begin{aligned}& M_o\ddot{x}_o + C_o\dot{x}_o + G_o - \tau_{ext} \\ &= \sum_{j=1}^{n} J_j\left(B_e\left(\dot{x}_{fj} - \dot{x}_o\right) + K_e\left(\delta_{fj}^o + x_{fj} - x_o\right)\right) \\ &= \sum_{j=1}^{n} J_j\left(B_e\dot{x}_{fj} + K_e\left(x_{fj} + \delta_{fj}^o\right)\right) - \Lambda\left(B_e\dot{x}_o + K_e x_o\right) \\ &= \sum_{j=1}^{n} J_j^x\left(B_e\dot{x}_{fj} + K_e\left(x_{fj} + \delta_{fj}^o\right)\right) - \Lambda\left(B_e\dot{x}_o + K_e x_o\right) + \sigma(x_o) \\ &= \sum_{j=1}^{n} Z_e J_j^x\left(x_{fj} + \delta_{fj}^o\right) - \Lambda\left(B_e\dot{x}_o + K_e x_o\right) + \sigma(x_o)\end{aligned}, \quad (5)$$

where $\Lambda = \sum_{j=1}^{n} J_j$, J_j^x is similar to J_j and calculated based on initial object positions and $\sigma(x_o)$ is a condensed expression of $\sum_{j=1}^{n}\left(J_j - J_j^x\right)\left(B_e\dot{x}_{fj} + K_e\left(x_{fj} + \delta_{fj}^o\right)\right)$.

Here, we move the terms corresponding to x_o from the right side of (5) to the left and define $\bar{\Phi}_o(x_o, \dot{x}_o, \ddot{x}_o)$ as a new hybrid object dynamics term as

$$\begin{aligned}\bar{\Phi}_o(x_o, \dot{x}_o, \ddot{x}_o) = M_o\ddot{x}_o + \bar{C}_o\dot{x}_o + \Lambda K_e x_o + G_o - \\ \tau_{ext} - \sigma(x_o)\end{aligned}, \quad (6)$$

where $\bar{C}_o = C_o + \Lambda B_e$ and then $\bar{\Phi}_o(x_o, \dot{x}_o, \ddot{x}_o)$ is expressed by a common impedance Z_e for all anticipating robots as

$$\bar{\Phi}_o(x_o, \dot{x}_o, \ddot{x}_o) = \sum_{j=1}^{n} Z_e J_j^x\left(x_{fj} + \delta_{fj}^o\right). \quad (7)$$

In the leader side, the dynamics of the object handled by all the manipulators is expressed by variables x_{lj}, δ_{lj}^o and contact force F_{ej}^v , $j = 1, 2, \ldots, n$ as

$$\begin{aligned}\bar{\Phi}_o(x_v,\dot{x}_v,\ddot{x}_v) &= \sum_{j=1}^{n} Z_e J_j^x \left(x_{lj}+\delta_{lj}^o\right) \\ &= \sum_{j=1}^{n} J_j^x F_{ej}^v - \left(Z_e J_j^x x_v \big|_{t=0^-}\right)\end{aligned} \quad (8)$$

where x_v represents the center position of the leader object, and F_{ej}^v is the force feedback to the operators, and δ_{lj}^o and x_v satisfying $\delta_{lj}^o = \delta_{fj}^o$ and $x_v\big|_{t=0^-} = x_o\big|_{t=0^-}$. On the leader side, the measured variables such as $x_v, \dot{x}_v, \ddot{x}_v$ and δ_{lj}^o etc. are converted to manipulation commands, which are subsequently transmitted to the follower side for robot control. There are two objectives for the multi-robot teleoperation:

1) Robots manipulate the object on the follower side to achieve the same effect as manipulating it with time delays on the leader side:

$$\begin{aligned}\bar{\Phi}_o(x_o,\dot{x}_o,\ddot{x}_o) &= \bar{\Phi}_o(x_v,\dot{x}_v,\ddot{x}_v)^{d(t)} \\ &= \sum_{j=1}^{n} J_j^x \left(B_e \dot{x}_{lj}^{d(t)} + K_e\left(x_{lj}^{d(t)}+\delta_{fj}^o\right)\right)\end{aligned} \quad (9)$$

2) For each follower robot, it is desired to track the motions of the corresponding leader : $x_{fj} = x_{lj}^{d(t)}, \dot{x}_{fj} = \dot{x}_{lj}^{d(t)}$.

Several assumptions, properties and lemmas are proposed as follows.

Assumption 1: During the manipulation, we only consider the deformation of the object δ_{fj}, and the rotation and slippage on the contact surface are not discussed.

Assumption 2 [20]: For every sampling time, the contact force is measured in a temporary stable state such that $\dot{F}_{ej}(k)=0$.

Assumption 3: There exist two positive parameters $p_{ij}^{\min}$ and $p_{ij}^{\max}, i=l,f$ satisfying $p_{ij}^{\min} \le \lambda_{\min}\left(M_{ij}^{-1}\right)$, $p_{ij}^{\max} \ge \lambda_{\max}\left(M_{ij}^{-1}\right)$.

Property 1**:** The matrix $\dot{M}_{ij} - 2C_{ij}$ in (1) is skew -symmetric.

Lemma 1: For any positive constant vector $k_b \in \Re^n$, the inequality holds for any vector $x \in \Re^n$ in the interval $|x| < |k_b|$

$$\log \frac{k_b^T k_b}{k_b^T k_b - x^T x} \le \frac{k_b^T k_b}{k_b^T k_b - x^T x}.$$

III. Controller Design

A. Error decomposition

To accomplish the above two control objectives, the follower robots need to maintain a balance between handling the object and control their own positions. This can be achieved by using (7) and (9), along with the definition of η_{fj} in Table 1, which provides a sufficient condition to achieve the desired object operational effect (Objective 1)

$$\sum_{j=1}^{n} J_j^x \eta_{fj} = 0, \quad (10)$$

and x_o in (7) is expressed by a nonlinear equation of $J_j^x x_{fj}$, $j=1,\dots,n$ as

$$x_o = f\left(J_1^x x_{f1}, J_2^x x_{f2}, \dots, J_n^x x_{fn}\right). \quad (11)$$

Taking (11) into the definition of F_{ek}, we can express F_{ek} as

$$\begin{aligned}F_{ek} &= B_e\left(\dot{x}_{fk} - \frac{df}{dt}\right) + K_e\left[x_{fk} - f\left(J_1^x x_{f1},\dots,J_n^x x_{fn}\right) + \delta_{fk}^o\right] \\ &= \sum_{j=1, j\ne k}^{n} \bar{B}_e\left(J_k^x \dot{x}_{fk} - J_j^x \dot{x}_{fj}\right) + \bar{K}_e\left(J_k^x x_{fk} - J_j^x x_{fj} + J_k^x \delta_{fk}^o\right) \\ &= \sum_{j=1, j\ne k}^{n} \bar{Z}_e\left(J_k^x x_{fk} - J_j^x x_{fj} + J_k^x \delta_{fk}^o\right)\end{aligned} \quad (12)$$

where $\bar{B}_e$ and $\bar{K}_e$ are equivalent varying stiffness and damping to B_e and K_e in (4), and $\bar{Z}_e$ is an equivalent impedance.

Furthermore, (10) can be expressed as

$$\sum_{j=1, j\ne k}^{n} \left(J_j^x \eta_{fj} - J_k^x \eta_{fk}\right) + nJ_k^x \eta_{fk} = 0. \quad (13)$$

If $x_{fj} = x_{lj}^{d(t)}, \dot{x}_{fj} = \dot{x}_{lj}^{d(t)}$ (Objective 2), that is if $\eta_{fk} = 0, \dot{\eta}_{fk} = 0$, $J_k^x \ne 0$, $k = 1,2,\dots,n$, we can get

$$\sum_{j=1, j\ne k}^{n} \left(J_j^x \eta_{fj} - J_k^x \eta_{fk}\right) = 0. \quad (14)$$

Taking $x_{lj}^{d(t)}, \dot{x}_{lj}^{d(t)}$ into (12), we get the desired contact force:

$$F_{ek}\left(x_{lj}^{d(t)}, \dot{x}_{lj}^{d(t)}\right) = \sum_{j=1, j\ne k}^{n} \bar{Z}_e\left(J_k^x x_{lk}^{d(t)} - J_j^x x_{lj}^{d(t)} + J_k^x \delta_{fk}^o\right), \quad (15)$$

and

$$\begin{aligned}&F_{ek}\left(x_{lj}^{d(t)}, \dot{x}_{lj}^{d(t)}\right) - F_{ek} \\ &= \bar{Z}_e \sum_{j=1, j\ne k}^{n} \left(J_k^x\left(x_{lk}^{d(t)} - x_{fk}\right) - J_j^x\left(x_{lj}^{d(t)} - x_{fj}\right)\right) \\ &= \bar{Z}_e \sum_{j=1, j\ne k}^{n} \left(J_k^x \eta_{fk} - J_j^x \eta_{fj}\right)\end{aligned} \quad (16)$$

Obviously, as $\bar{Z}_e$ is not always zero, the stability conditions in (14) and (16) are equal, which means that if the force exerted by each robot matches the force commands from the leader side, the object will be manipulated in a same state to the leader side (Objective 1). Additionally, if (14) and (10) are satisfied, we have $F_{ek}\left(x_{lj}^{d(t)}, \dot{x}_{lj}^{d(t)}\right) = F_{ek}$, $\eta_{fk} = 0$, and $\dot{\eta}_{fk} = 0$, which means that the position errors will decrease to 0 at the final steady state. Following (10) and (14), we define two new error terms:

$$\begin{aligned}&\eta_f^C = \sum_{j=1}^{n} J_j^x \eta_{fj}, \eta_{fk}^D = J_k^x \eta_{fk} - \frac{1}{n}\eta_f^C, \\ &\eta_f^D = \left[\eta_{f1}^D, \eta_{f2}^D \dots, \eta_{fn}^D\right]^T\end{aligned} \quad (17)$$

where η_f^C corresponds with the object dynamics in (9) and η_{sk}^D relates to the independent robot operational effect in (12). Then, the error term can be expressed by $\eta_{fk}, k=1,\dots,n$ as

$$\begin{bmatrix} \eta_f^C \\ \eta_f^D \end{bmatrix} = \mathbf{N}\boldsymbol{\eta}_f = \begin{bmatrix} J_1^x & J_2^x & \cdots & J_n^x \\ \frac{(n-1)J_1^x}{n} & -\frac{J_2^x}{n} & \cdots & -\frac{J_n^x}{n} \\ \vdots & \vdots & \ddots & \vdots \\ -\frac{J_1^x}{n} & -\frac{J_2^x}{n} & \cdots & \frac{(n-1)J_n^x}{n} \end{bmatrix} \begin{bmatrix} \eta_{f1} \\ \eta_{f2} \\ \vdots \\ \eta_{fn} \end{bmatrix} \quad (18)$$

Remark 1: Eq.(18) is similar to the decomposition approach utilized in a single-leader multi-follower (SLMF) teleoperation for multiple robots, ensuring the system's passivity and stability [28]–[30]. In passive decomposition, the dynamics of multiple robots are split into a shape system and a blocking system. The shape system characterizes the internal formation of the robots, while the blocking system describes the collective movement and center of gravity behavior, replicating the leader's actions.

Similarly, in (18), the η_f^C is used to minimize the dynamics tracking errors of the object, resembling the blocking system in the single-leader multi-follower (SLMF) teleoperation. The η_{fk}^D is similar to the shape system by distributing $1/n$ the common object operational effect based on position tracking error $J_k^x \eta_{fk}$ of each robot. The error matrix in (18) serves an inspiration for the development of a hierarchical controller for the teleoperation system in this paper. As shown in Fig. 1, the inner layer firstly constructs an object observer to minimizes dynamics tracking errors, as described in Section III.B. This is followed by the outer layer, which aims to reduce the position and force tracking errors of each robot based on the observation of inner layer and an improved BLFs method.

B. Object state observer

Following (7) and (12), we have

$$\begin{aligned} F_{ek} &= (n-1)\bar{Z}_e J_k^x \left(x_{fk} + \delta_{fk}^o\right) - \bar{Z}_e \sum_{j=1, j\neq k}^{n} J_j^x x_{fj} \\ &= n\bar{Z}_e J_k^x \left(x_{fk} + \delta_{fk}^o\right) - \bar{Z}_e \left(\frac{\bar{\Phi}_o}{Z_e} - \sum_{j=1}^{n} J_j^x \delta_{fj}^o \right), \\ &= \bar{Z}_e \left(\sum_{j=1}^{n} \left(J_k^x \left(x_{fk} + \delta_{fk}^o\right) + J_j^x \delta_{fj}^o \right) - \frac{\bar{\Phi}_o}{Z_e} \right) \end{aligned} \quad (19)$$

where $\bar{Z}_e$ is a varying term that is equivalent to Z_e of the kth robot. Eq. (19) connects F_{ek} and $\bar{\Phi}_o(x_o, \dot{x}_o, \ddot{x}_o)$ through $\bar{Z}_e$. We consider the time delay μ in a local communication loop. Using (12), the factors $\bar{B}_e$ and $\bar{K}_e$ in $\bar{Z}_e(t)$ are estimated by

$$\begin{cases} \bar{B}_e = \left(J_k^x\right)^{-1} B_e \big/ (n-1) \\ \bar{K}_e = \dfrac{\hat{F}_{ek} - \bar{B}_e \dot{x}_{fk}}{\sum\limits_{j=1, j\neq k}^{n} \left(J_k^x x_{fk} - J_j^x x_{fj}\big|_{t-\mu} + J_k^x \delta_{fk}^o \right)} \end{cases}. \quad (20)$$

Remark 2: Factors B_e and K_e in (4) are constants, whereas in (20), $\bar{B}_e$ and $\bar{K}_e$ are time-varying and have multiple values for the same $\hat{F}_{ek}$. In addition, the velocities in (20) are treated as transient variables, and signals transmitted from neighbouring robots introduce errors due to local time delays, denoted as μ . Under the statement in Assumption 2, the contact force $\hat{F}_{ek}$ are estimated in a stable manner. Therefore, we compute $\bar{B}_e$ for the kth robot in (20) first. Next, the unique $\bar{K}_e$ is achieved by disregarding the velocity terms of other coordinators. Finally, as we achieve $\bar{B}_e$ and $\bar{K}_e$, the value of $\hat{F}_{ek}$ can converge to the real value F_{ek} gradually.

Remark 3: In (20), we incorporate $J_j^x x_{fj}\big|_{t-\mu}$ as delayed terms in the estimation of $\bar{K}_e$. The factors $\bar{B}_e$ and $\bar{K}_e$ are calculated using the measurements x_{fk} and $\dot{x}_{fk}$ along with the estimation $\hat{F}_{ek}$ of the kth robot, which reflects the overall perception of the manipulation situation for the kth robot. It is worth noting that these factors may vary among robots, as each robot may have a distinct perception of the manipulation situation.

According to Assumption 2, we have $\dot{\hat{F}}_{ej} + \dot{\tilde{F}}_{ej} = \dot{F}_{ej} = 0$, the contact force is then estimated by

$$\begin{aligned} \dot{\hat{F}}_{ek} = L\hat{F}_{ek} - LJ_{fk}^{-1}(q_{fk})\big[\tau_{fk} - M_{fk}\left(q_{fk}\right)\ddot{q}_{fk} - \\ C_{fk}\left(q_{fk}, \dot{q}_{fk}\right)\dot{q}_{fk} - G_{fk} \big] \end{aligned}, \quad (21)$$

where L is a high-gain positive matrix. Taking (19) into (21) , we can deduce the estimation of $\bar{\Phi}_o$ as

$$\begin{aligned} \dot{\hat{\Phi}}_o = L\hat{\Phi}_o - LZ_e \sum_{j=1}^{n} \left(J_k^x \left(x_{fk} + \delta_{fk}^o \right) + J_j^x \delta_{fj}^o \right) + \\ nZ_e \left(J_k^x \dot{x}_{fk} + \dot{J}_k^x x_{fk} \right) + \frac{LZ_e}{\bar{Z}_e} J_{fk}^{-1}(q_{fk}) \bullet \\ \left[\tau_{fk} - M_{fk}\left(q_{fk}\right)\ddot{q}_{fk} - C_{fk}\left(q_{fk}, \dot{q}_{fk}\right)\dot{q}_{fk} - G_{fk} \right] \end{aligned}. \quad (22)$$

Taking $\dot{\hat{F}}_{ek} + \dot{\tilde{F}}_{ek} = 0$ and $\hat{F}_{ek} + \tilde{F}_{ek} = F_{ek}$ into (21), we have $\dot{\tilde{F}}_{ek} = -L\tilde{F}_{ek}$, then the estimation error $\tilde{F}_{ek}$ will converge to 0 finally. Here, we set the value of $\tilde{F}_{ek}$ is bounded with $\|\tilde{F}_{ek}\| \le \sigma_e$ in stable, then $\hat{\Phi}_o$ derived from $\hat{F}_{ek}$ is bounded with $\|\tilde{\Phi}_o\| \le \sigma_o$.

C. Follower controller design

According to Fig. 1, the control torque τ_{fk} of the kth robot contains three parts:

$$\tau_{fk} = \tau_{fk}^f + \tau_{fk}^p + \tau_{fk}^{dyn}, \quad (23)$$

where τ_{fk}^f is to control the object's manipulation performance, τ_{fk}^p enables a robot to track its own prescribed performance and address unknown disturbing force/torque errors caused by τ_{fk}^f , and τ_{fk}^{dyn} is to deal with robot dynamics terms and errors. The similar control structure is also shown in [21], [22]. The three terms in (23) are introduced separately in the following content.

1) Term τ_{fk}^{f}

After acquiring $\hat{\Phi}_o$ and $\hat{F}_{ek}$, we can build the term τ_{fk}^{f} to deal with the outer contact forces F_{ek}

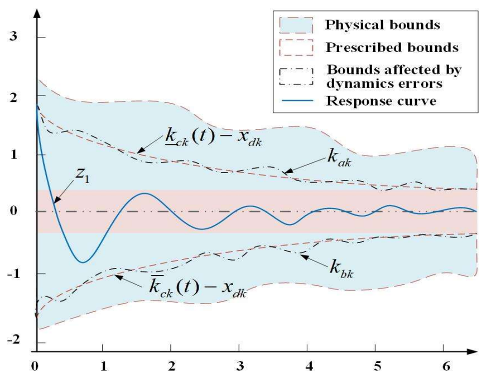

Fig. 3. Three constrains for robot performance control.

$$\begin{aligned}\tau_{fk}^{f} &= J_{fk}^{T}(q_{fk})\hat{F}_{ek} \\ &= J_{fk}^{T}(q_{fk})\bar{Z}_{ek}\left(\sum_{j=1}^{n}\left(J_{k}^{x}\left(x_{fk}+\delta_{fk}^{o}\right)+J_{j}\delta_{fj}^{o}\right)-\frac{\hat{\Phi}_o}{Z_e}\right)\end{aligned} .(24)$$

To minimize the dynamics estimation errors of the object on the follower side to match those on the leader side, we add an new term to (24) and the expression of τ_{fk}^{f} is represented as

$$\begin{aligned}\tau_{fk}^{f} = J_{fk}^{T}(q_{fk})\bar{Z}_{ek}\left(\sum_{j=1}^{n}\left(J_{k}^{x}\left(x_{fk}+\delta_{fk}^{o}\right)+J_{j}^{x}\delta_{fj}^{o}\right)-\frac{\hat{\Phi}_o}{Z_e}\right)+ \\ k_w\omega_k\left(\hat{\Phi}_o-\Phi_o^d(x_v^{d(t)},\dot{x}_v^{d(t)},\ddot{x}_v^{d(t)})\right)\end{aligned} ,(25)$$

where k_w is a constant and ω_k is a constant factor sharing the dynamics error with $\sum_{j=1}^{n}\omega_j=1$. Usually, $\omega_k=1/n$ is to match the error divisions in (18) and then the estimation error term is bounded with

$$\begin{aligned}\left\|J_{fk}^{T}(q_{fk})\tilde{F}_{ek}+k_1\omega_k\tilde{\Phi}_o\right\| &\le \left\|J_{fk}^{T}(q_{fk})\right\|\left\|\tilde{F}_{ek}\right\|+k_w\omega_k\left\|\tilde{\Phi}_o\right\| \\ &\le \alpha_f\left\|\tilde{F}_{ek}\right\|+k_w\omega_k\left\|\tilde{\Phi}_o\right\| \\ &\le \alpha_f\sigma_e+k_w\omega_k\sigma_o=\Delta_{fk}\end{aligned} ,(26)$$

where α_f is a bounded number satisfying $\left\|J_{fk}^{T}(q_{fk})\right\|<\alpha_f$.

2) Term τ_{fk}^{p}

BLFs is a kind of candidate that imposes constraints on the system's output states [33]. Previous research on BLFs mostly focused on the constraints such as input saturation, and utilized neural networks (NNs) to approximate and compensate them [31], [34]. In this paper, we consider three kinds of constraints as shown in Fig.3. The outermost constraints are determined by physical conditions, for example, to prevent object falling down, the object deformation must satisfy $\delta_{fk}=\delta_{fk}^{o}+x_{fk}-x_o>0$. The innermost constrain aims to limit the position/velocity tracking errors within desired prescribed performance bounds similar to the approach in [31] and [34]. Additionally, we considered the dynamics estimation errors $\hat{\Phi}_o-\Phi_o^d$, which impact the position tracking performance. To address this, we introduce a new term Δx_k to the innermost layer:

$$\Delta x_k = J_{fk}^{-1}(q_{fk})\frac{\Phi_o^d(x_v^{d(t)},\dot{x}_v^{d(t)},\ddot{x}_v^{d(t)})-\hat{\Phi}_o(x_o,\dot{x}_o,\ddot{x}_o)}{n\min\left(\bar{Z}_e\right)} ,(27)$$

where Δx_k is calculated by the minimum value of $\bar{Z}_e$ in history.

Define $x_{1k}=q_{fk}$, $x_{2k}=\dot{q}_{fk}$, $x_{dk}=q_{lk}^{d(t)}$, and q_{fk} is required to satisfy joint constrains as

$$\underline{k}_{ck}(t)<q_{fk}<\bar{k}_{ck}(t),\ \forall t>0 \quad (28)$$

Set new variables $z_{1k}=x_{1k}-x_{dk}$ and $z_{2k}=x_{2k}-\alpha_k$, α_k is a virtual controller function expressed by

$$\alpha_k=\dot{x}_{dk}-k_1z_{1k}-K_kz_{1k} . \quad (29)$$

Set the outermost constraints of q_{fk} as $\left[\underline{k}_{pk}(t),\bar{k}_{pk}(t)\right]$, then the time-varying barriers for z_1 are given by

$$\begin{cases}k_{ak}:=\min\left(\underline{k}_{ck}(t)-x_{dk}-\left|\Delta x_k\right|,\underline{k}_{pk}(t)-x_{dk}\right) \\ k_{bk}:=\max\left(\bar{k}_{ck}(t)-x_{dk}+\left|\Delta x_k\right|,\bar{k}_{pk}(t)-x_{dk}\right)\end{cases} \quad (30)$$

and τ_{fk}^{p} is designed as

$$\tau_{fk}^{p}=M_{fk}\left[\ddot{x}_{dk}-f\left(z_{1k}\right)+\left(\left(k_1+K_k\right)^2-1\right)z_{1k}-\left(k_1+K_k+\bar{k}\right)z_{2k}\right] \quad (31)$$

where $K_k=\sqrt{\left(\frac{\dot{k}_{ak}}{k_{ak}^2}\right)^2+\left(\frac{\dot{k}_{bk}}{k_{bk}^2}\right)^2+\beta}$, and β and k_1 are positive factors, and $\bar{k}>\Delta_{fk}p_{ij}^{\max}/\mu_{fk}$, and μ_{fk} is a positive number.

3) Term τ_{fk}^{dyn}

The τ_{fk}^{dyn} in (23) is designed as

$$\tau_{fk}^{dyn}=C_{fk}\left(q_{fk},\dot{q}_{fk}\right)\dot{q}_{fk}+G_{fk}+\sigma_{fk} . \quad (32)$$

where σ_{fk} is a robust term

$$\begin{aligned}\sigma_{fk} &= \Delta_{fk}sat(z_{2k},\mu_{fk}) \\ sat(z_{2k},\mu_{fk}) &= \begin{cases}1 & z_{2k}>\mu_{fk} \\ z_{2k}/\mu_{fk} & -\mu_{fk}<z_{2k}<\mu_{fk} \\ -1 & z_{2k}<-\mu_{fk}\end{cases}\end{aligned} , \quad (33)$$

where μ_{fk} and z_{2k} are presented in (31) .

D. Leader controller design

The leader controller is designed with a different purpose to the follower controller that is to minimize the position tracking errors between the leader and follower side . The controller τ_{lk} in (1) is built as

$$\begin{aligned}\tau_{lk} = -M_{lk}\left(q_{lk}\right)\left(\ddot{q}_{lk}^{d}+k_2\dot{e}_{lk}\right)-C_{lk}\left(\dot{q}_{lk},q_{lk}\right)\left(\dot{q}_{lk}^{d}+k_2e_{lk}\right)+ \\ G_{lk}-J_{lk}^{T}(q_{lk})F_{hk}^{p}+\sigma_{lk}+k_3r_{lk}\end{aligned} ,(34)$$

where $r_{lk} = \dot{e}_{lk} + k_2 e_{lk}$, k_2 is a constant, and F_{hk}^p is the force to enable the leaders to move along x_{lk}^p with a boundary of F_{hk}^{bound} as

$$\left\| F_{hk} - F_{hk}^p \right\| \le F_{hk}^{bound}, \tag{35}$$

and σ_{lk} is a robust item to counteract the error $F_{hk} - F_{hk}^p$ as

$$\sigma_{lk} = \alpha_l F_{hk}^{bound} sat(r_{lk}, \mu_{lk})$$
$$sat(r_{lk}, \mu_{lk}) = \begin{cases} 1 & r_{lk} > \mu_{lk} \\ r_{lk}/\mu_{lk} & -\mu_{lk} < r_{lk} < \mu_{lk} \\ -1 & r_{lk} < -\mu_{lk} \end{cases}, \tag{36}$$

where μ_{lk} is a positive bounding number and α_l satisfies that $\left\| J_{lk}^T(q_{lk}) \right\| < \alpha_l$, and k_3 is a positive constant.

IV. Stability Analysis

Theorem 1: For the multi-robot teleoperation system defined in (1), with controllers (23) and (34) , given initial conditions $\underline{k}_{aj}(0) \le \eta_{fj}(0) \le \overline{k}_{bj}(0)$, the proposed control scheme in Fig.1 ensures the following properties.

1) The cooperative robots can manipulate the object with the desired dynamics Φ_o^d;

2) Tracking errors e_{fj} of the follower robots are bounded by predefined boundaries k_{ak} and k_{bk};

3) Tracking errors e_{lj} of the leader manipulators are uniformly ultimately bounded and converged.

Proof. Consider the following Lyapunov function:

$$\begin{aligned} V &= V_f + V_l, \\ V_f &= \sum_{k=1}^n V_{fk} = \sum_{k=1}^n \left(V_k + \frac{1}{2}\left(z_{1k}^2 + z_{2k}^2\right)\right), \\ V_k &= \frac{q}{2p}\log\frac{k_{bk}^{2p}(t)}{k_{bk}^{2p}(t) - z_{1k}^{2p}} + \frac{1-q}{2p}\log\frac{k_{ak}^{2p}(t)}{k_{ak}^{2p}(t) - z_{1k}^{2p}}, \\ V_l &= \sum_{k=1}^n V_{lk} = \frac{1}{2}\sum_{k=1}^n r_{lk}^T M_{lk} r_{lk}, \end{aligned} \tag{37}$$

where p is a positive integer and q is a threshold factor that $q=1$, if $z_{1k} > 0$ and $q=0$, if $z_{1k} \le 0$. Let $\xi_{ak} = \frac{z_{1k}}{k_{ak}}$, $\xi_{bk} = \frac{z_{1k}}{k_{bk}}$, $\xi_k = q\xi_{bk} + (1-q)\xi_{ak}$, then V_k in (37) can be rewritten as

$$V_k = \frac{1}{2p}\log\frac{1}{1-\xi_k^{2p}}. \tag{38}$$

The differentiable function of V_k is

$$\dot{V}_k = \frac{1}{2p}\left(1-\xi_k^{2p}\right)\frac{2p\xi_k^{2p-1}\dot{\xi}_k}{\left(1-\xi_k^{2p}\right)^2} = \frac{\xi_k^{2p-1}\dot{\xi}_k}{1-\xi_k^{2p}}, \tag{39}$$

and the differentiable function of ξ_k is

$$\begin{aligned} \dot{\xi}_k &= q\dot{\xi}_{bk} + (1-q)\dot{\xi}_{ak} \\ &= q\frac{\dot{z}_{1k}k_{bk} - z_{1k}\dot{k}_{bk}}{\left(k_{bk}\right)^2} + (1-q)\frac{\dot{z}_{1k}k_{ak} - z_{1k}\dot{k}_{ak}}{\left(k_{ak}\right)^2} \\ &= q\left[\frac{x_{2k} - \dot{x}_{dk}}{k_{bk}} - \frac{z_{1k}}{k_{bk}^2}\dot{k}_{bk}\right] + (1-q)\left[\frac{x_{2k} - \dot{x}_{dk}}{k_{ak}} - \frac{z_{1k}}{k_{ak}^2}\dot{k}_{ak}\right] \end{aligned}. \tag{40}$$

Substitute (40) to (39) and use $x_{2k} = z_{2k} + \alpha_k$, then $\dot{V}_k$ is expressed as

$$\begin{aligned} \dot{V}_k &= \frac{q\xi_{bk}^{2p-1}}{k_{bk}\left(1-\xi_{bk}^{2p}\right)}\left[z_{2k} + \alpha_k - \dot{x}_{dk} - z_{1k}\frac{\dot{k}_{bk}}{k_{bk}}\right] + \frac{(1-q)\xi_{ak}^{2p-1}}{k_{ak}\left(1-\xi_{ak}^{2p}\right)} \\ &\quad \left[z_{2k} + \alpha_k - \dot{x}_{dk} - z_{1k}\frac{\dot{k}_{ak}}{k_{ak}}\right] \\ &= \frac{qz_{1k}^{2p-1}}{k_{bk}^{2p} - z_{1k}^{2p}}\left[z_{2k} + \alpha_k - \dot{x}_{dk} - z_{1k}\frac{\dot{k}_{bk}}{k_{bk}}\right] + \frac{(1-q)z_{1k}^{2p-1}}{k_{ak}^{2p} - z_{1k}^{2p}} \\ &\quad \left[z_{2k} + \alpha_k - \dot{x}_{dk} - z_{1k}\frac{\dot{k}_{ak}}{k_{ak}}\right] \\ &= \frac{qz_{1k}^{2p-1}z_{2k}}{k_{bk}^{2p} - z_{1k}^{2p}} + \frac{qz_{1k}^{2p-1}}{k_{bk}^{2p} - z_{1k}^{2p}}\left[\alpha_k - \dot{x}_{dk} - z_{1k}\frac{\dot{k}_{bk}}{k_{bk}}\right] + \\ &\quad \frac{(1-q)z_{1k}^{2p-1}z_{2k}}{k_{ak}^{2p} - z_{1k}^{2p}} + \frac{(1-q)z_{1k}^{2p-1}}{k_{ak}^{2p} - z_{1k}^{2p}}\left[\alpha_k - \dot{x}_{dk} - z_{1k}\frac{\dot{k}_{ak}}{k_{ak}}\right] \end{aligned} .\tag{41}$$

Define $K_k = \sqrt{\left(\frac{\dot{k}_{ak}}{k_{ak}}\right)^2 + \left(\frac{\dot{k}_{bk}}{k_{bk}}\right)^2 + \beta}$, β is a positive number, then the following inequalities hold

$$-K_k - \frac{\dot{k}_{ak}}{k_{ak}} < 0; \ -K_k - \frac{\dot{k}_{bk}}{k_{bk}} < 0. \tag{42}$$

Then taking (29) into (41) ,we have

$$\begin{aligned} \dot{V}_k &= \left[\frac{qz_{1k}^{2p-2}}{k_{bk}^{2p} - z_{1k}^{2p}} + \frac{(1-q)z_{1k}^{2p-2}}{k_{ak}^{2p} - z_{1k}^{2p}}\right]\left(z_{1k}z_{2k} - k_1 z_{1k}^2\right) + \\ &\quad \frac{qz_{1k}^{2p}}{k_{bk}^{2p} - z_{1k}^{2p}}\left(-K_k - \frac{\dot{k}_{bk}}{k_{bk}}\right) + \frac{(1-q)z_{1k}^{2p}}{k_{ak}^{2p} - z_{1k}^{2p}}\left(-K_k - \frac{\dot{k}_{ak}}{k_{ak}}\right) \\ &\le \left[\frac{qz_{1k}^{2p-2}}{k_{bk}^{2p} - z_{1k}^{2p}} + \frac{(1-q)z_{1k}^{2p-2}}{k_{ak}^{2p} - z_{1k}^{2p}}\right]\left(z_{1k}z_{2k} - k_1 z_{1k}^2\right) \\ &= f\left(z_{1k}\right)z_{2k} - k_1\frac{1}{1-\xi_k^{2p}} \end{aligned} .\tag{43}$$

where $f\left(z_{1k}\right) = \left[\frac{qz_{1k}^{2p-1}}{k_{bk}^{2p} - z_{1k}^{2p}} + \frac{(1-q)z_{1k}^{2p-1}}{k_{ak}^{2p} - z_{1k}^{2p}}\right]$ is a function about z_{1k}.

The differentiable function of V_{fk} is

$$\dot{V}_{fk} = \dot{V}_k + z_{1k}\dot{z}_{1k} + z_{2k}\dot{z}_{2k}, \tag{44}$$

where $z_{1j}\dot{z}_{1j}$ and $z_{2j}\dot{z}_{2j}$ are calculated by

$$\begin{cases} z_{1k}\dot{z}_{1k} = z_{1k}\left(x_{2k}-\dot{x}_{dk}\right) \\ \qquad = z_{1k}\left(z_{2k}+\alpha_k-\dot{x}_{dk}\right) \\ \qquad = z_{1k}z_{2k}-\left(k_1+K_k\right)z_{1k}^2 \\ z_{2k}\dot{z}_{2k} = z_{2k}\left(\dot{x}_{2k}-\dot{\alpha}_k\right) \\ \qquad = z_{2k}\left(\dot{x}_{2k}-\ddot{x}_{dk}+\left(k_1+K_k\right)\dot{z}_{1k}\right) \end{cases}. \tag{45}$$

Meanwhile, taking the controller (23) into (1), we have

$$\begin{aligned}\dot{x}_{2k}-\ddot{x}_{dk} = &\left(\left(k_1+K_k\right)^2-1\right)z_{1k}-\left(k_1+K_k+\bar{k}\right)z_{2k}- \\ &f\left(z_{1k}\right)+M_{fk}^{-1}\left(J_{fk}^T(q_{fk})\tilde{F}_{ek}+k_w\omega_k\tilde{\Phi}_o-\sigma_{fk}\right)\end{aligned}. \tag{46}$$

Taking (46) and (45) into (44), we get

$$\begin{aligned}\dot{V}_{fk} \le\, & f\left(z_{1k}\right)z_{2k}-k_1\frac{1}{1-\xi_k^{2p}}+z_{1k}z_{2k}-\left(k_1+K\right)z_{1k}^2+ \\ & z_{2k}\left(\dot{x}_{2k}-\ddot{x}_{dk}+\left(k_1+K\right)\dot{z}_{1k}\right) \\ = & f\left(z_{1k}\right)z_{2k}-k_1\frac{1}{1-\xi_k^{2p}}+z_{1k}z_{2k}-\left(k_1+K\right)z_{1k}^2+ \\ & z_{2k}\Big[-f\left(z_{1k}\right)+\left(k_1+K\right)\left(z_{2k}-\left(k_1+K\right)z_{1k}\right)+ \\ & \left(\left(k_1+K\right)^2-1\right)z_{1k}-\left(k_1+K_k+\bar{k}\right)z_{2k}+ \\ & M_{fk}^{-1}\left(J_{fk}^T(q_{fk})\tilde{F}_{ek}+k_w\omega_k\tilde{\Phi}_o-\sigma_{fk}\right)\Big] \\ = & -k_1\frac{1}{1-\xi_k^{2p}}-\left(k_1+K\right)z_{1k}^2-\bar{k}z_{2k}^2+ \\ & M_{fk}^{-1}\left(J_{fk}^T(q_{fk})\tilde{F}_{ek}+k_w\omega_k\tilde{\Phi}_o-\sigma_{fk}\right)z_{2k} \\ \le & -k_1\frac{1}{1-\xi_k^{2p}}-\left(k_1+K\right)z_{1k}^2-\left(\bar{k}-\Delta_{fk}p_{fk}^{\max}/\mu_{fk}\right)z_{2k}^2\end{aligned}. \tag{47}$$

The differential of V_{lk} is

$$\dot{V}_{lk} = r_{lk}^T M_{lk}\dot{r}_{lk}+r_{lk}^T\dot{M}_{lk}r_{lk}/2\,. \tag{48}$$

Take the controller (34) into (1), we have

$$\begin{aligned}M_{lk}(q_{lk})\dot{r}_{lk} = & -C_{lk}\left(\dot{q}_{lk},q_{lk}\right)r_{lk}+J_{mj}^T(q_{lk})\left(F_{hk}-F_{lk}^p\right)+ \\ & \alpha_l F_{hk}^{bound}.sat\left(r_{lk},\mu_{lk}\right)-k_3 r_{lk}\end{aligned}. \tag{49}$$

Substitute (49) into (48) and utilize Property 1, we get

$$\dot{V}_{lk} = r_{lk}^T\left[J_{lk}^T(q_{lk})\left(F_{hk}-F_{hk}^p\right)+\sigma_{lk}\right]-k_3 r_{lk}^T r_{lk}\,. \tag{50}$$

Since $\left\|J_{lk}^T(q_{lk})\left(F_{hk}-F_{hk}^p\right)\right\| < \left\|J_{lk}^T(q_{lk})\right\|\left\|F_{hk}-F_{hk}^p\right\| < \alpha_l F_{hk}^{bound}$, and following (36), we have

$$\dot{V}_{lk} \le -k_3 r_{lk}^T r_{lk}\,. \tag{51}$$

Define $p_f^{\max} = \min\left(p_{fj}^{\max}\right), j=1,2,\ldots,n$, the differential of V is given by

$$\begin{aligned}\dot{V} &= \dot{V}_f+\dot{V}_l \\ &\le \sum_{k=1}^{n}\Bigg(-k_1\frac{1}{1-\xi_k^{2p}}-\left(\bar{k}-\Delta_{fk}p_f^{\max}/\mu_{fk}\right)z_{2k}^2- \\ &\qquad \left(k_1+K\right)z_{1k}^2\Bigg)-k_3\sum_{k=1}^{n}r_{lk}^T r_{lk}\end{aligned}. \tag{52}$$

Following Assumption 3, we define $p_l^{\min} = \min\left(p_{lj}^{\min}\right) \le \lambda_{\min}\left(M_{lj}^{-1}\right), j=1,2,\ldots,n$, then it is given by

$$\begin{aligned}\dot{V}_l &\le -k_3\sum_{k=1}^{n}r_{lk}^T r_{lk} < -k_3\sum_{k=1}^{n}p_{lk}^{\min}r_{lk}^T M_{lk}r_{lk} \\ &< -k_3 p_l^{\min}\sum_{k=1}^{n}r_{lk}^T M_{lk}r_{lk} \\ &= -2k_3 p_l^{\min}V_l\end{aligned}. \tag{53}$$

Following Lemma 1, the inequality (52) can be represented as

$$\dot{V} \le -\zeta V\,, \tag{54}$$

Where $\zeta = \min\left(2(K+k_1), 2(\bar{k}-\Delta_{fk}p_f^{\max}/\mu_{fk}), 2k_3 p_l^{\min}\right)$.

Multiply both sides by $e^{\zeta t}$ in (54), and apply the integration over $[0,t]$, we have

$$V(t) \le V(0)e^{-\zeta t}\,. \tag{55}$$

Seen from inequality (55), we can get the terms $\log\frac{1}{1-\xi^{2p}}$ along with the leader and follower position tracking errors, are bounded. This concludes the proof.

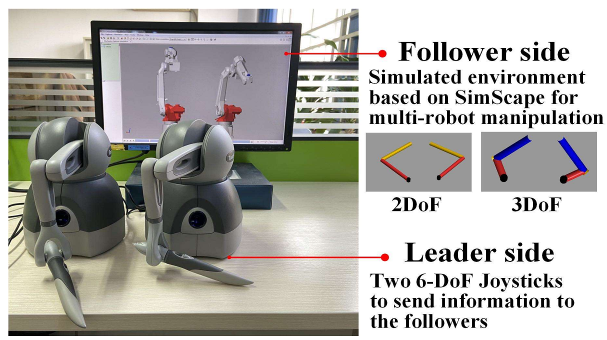

Fig. 4. Experimental setups.

TABLE II.
VALUES FOR SYMBOLS

Symbol	Values	Symbol	Values
M_o	1kg	F_{hj}^{bound}	1
B_e	2kg.s^{-1}	k_2	diag([4.1,4.4])
K_e	50kg.s^{-2}	$\bar{k}$	1
δ_{fj}^o	0.3m	k_3	diag(5,5)
L	-20	L_{k1}, L_{k2}	0.3m
Δ_{fk}	0.3	a_{k1}, a_{k2}	0.1m
ω_1, ω_2	0.5	m_{f1}, m_{f2}	0.23 kg, 0.46kg
k_1	1	m_{l1}, m_{l2}	0.12 kg, 0.14kg
p	1	I_{f1}, I_{f2}	0.03 kgm^2,0.06 kgm^2
α_f, α_l	0.5	I_{l1}, I_{l2}	0.01 kgm^2,0.02 kgm^2

V. EXPERIMENTS

In the real world, direct measurement of the deformation and the centre position of the object is not possible. Therefore, the leading manipulators utilize virtual contact forces to provide feedback to human operators. These forces are calculated using the Robotics Toolbox for Education (ARTE) [35], along with models of the robot arms and the object, which are simulated using SimScape/Matlab in Fig.4. The physical leading side is equipped with two Omni Phantom joysticks, which enable the capture of human motions and provide timely force feedback to the operator's hands.

The parameters of the virtual multi-robots on the following side are shown in Table II, along with the factors of the virtual object. Some of the symbols are: $L_{ij}, m_{ij}, i = l, f; j = 1,2$ are the lengths and masses of the links of robots or manipulator , I_{lj} and $I_{fj}, j = 1,2$ are the inertia moments of the robots or manipulator of humans. The rest parameters in Table II of the robots and the manipulators are introduced in the previous context.

We set the time delay along the communication channels as:

$$d(t) = 0.25 + 0.1\sin(t) + 0.14\sin(2t) \tag{56}$$

Two leading manipulators are operated by humans to move along the trajectories:

$$left: \begin{cases} x = 0.2\sin(t) + 0.1 \\ y = 0.3 \end{cases} \quad right: \begin{cases} x = 0.2\sin(t) - 0.1 \\ y = 0.3 \end{cases} \tag{57}$$

To evaluate the effectiveness of the proposed control scheme for cooperative multi-robot teleoperation, we build a controller described in [22],[23] and compare the operational performance with that of the proposed method. The controller is defined as follows:

$$\begin{aligned} \tau_{fk} = -M_{fk}\left(q_{fk}\right)\dot{r}_{fk} + C_{fk}\left(\dot{q}_{fk}, q_{fk}\right)r_{fk} + G_{fk} + \\ J_{fk}^{T}(q_{fk})\hat{F}_{ej} \end{aligned}, \tag{58}$$

where $r_{fk} = \dot{q}_{fk} + k_2 e_{fk}$, and k_2 is a constant gain and $\hat{F}_{ej}$ is the environmental contact force estimated by (21). The leaders use the same controllers as in (34). Then, we conduct the following experiments to compare the two control schemes. In subsection A, we compare position and force tracking errors of robots to the leaders commands. In subsection B, we impose a disturbing force $\Delta F = 4N$ on the object for a time period and compare the movement of the object centre. In subsection C, we investigate that if the position tracking errors remain within the prescribed bounds.

A. Position and force tracking performance

Fig.5 (a) illustrates the desired and the actual trajectories of robots. Fig.5 (c) presents the contact forces applied to the object by the robot ends using controllers (23) and (34). Fig.5 (b) and (d) are the comparative results using controllers (58) and (34). The results show that proposed control scheme takes slightly longer (about 3s) to reduce the absolute tracking error of the robots to 0.02m. Controller (58) achieves this in less time (2.4s) but with larger trajectory fluctuations during the initial stage (0s -2.4s) and larger tracking errors during the target approaching progress, as shown in Fig. 5(e). These fluctuations affect not only the object state (Fig. 5(b)), but also the contact forces (Fig. 5(d)). Furthermore, the contact forces applied by controller (34) increase smoothly from 0 to around 10N and maintain a small fluctuation as the object motion progresses (Fig. 5(c)). However, controller (58) generates large force oscillations, which are up to a maximum of 15N, which is caused by interactions between

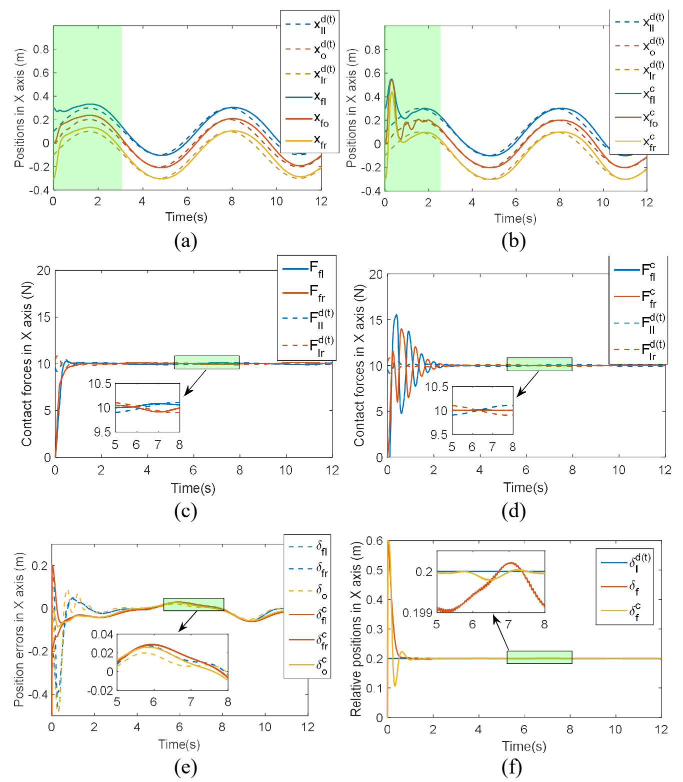

Fig. 5. Trajectories of leaders, followers and object and contact forces on the robot ends of proposed method ((23) and (34),) and comparative method ((58) and (34)) **(a)** Positions of the proposed methods; **(b)** Positions of the comparative methods; **(c)** Contact forces of the proposed methods; **(d)** Contact forces of the comparative methods; **(e)** Position tracking errors of two methods **(f)** Relative positions of two leading manipulators/following robot end effectors of two methods.

the robots and the damped shaking of the object.

In addition, we choose the relative distance as a standard to evaluate the cooperative manipulation as described in [22]. Fig. 5(f) illustrates that the desired displacement is 0.2 m and our proposed controllers enable the robots to approach this value uniformly. However, controller (58) leads to an overshoot, decreasing the minimum value to about 0.1 m, which could probably damage the object and the robots. Fig.5 (f) shows that the relative distance errors in the steady state of the proposed controllers are slightly larger than those of controller (58), but both remain smaller than 0.001m.

B. Disturbance recovering performance

To investigate the robustness of the two methods, an external force $\Delta F = 4N$ is applied to the object between 5 s and 5.8 s (highlighted in red in Fig. 6 (a) to Fig. 6 (d)), while the green areas represent the process of state recovery. The images in Fig.6 correspond to the same experimental conditions as those from Fig.5 (a) to (d), but with the addition of the external force. After 5s, the system reached a stable state and was disrupted by the external force ΔF. This led to changes in the positions and velocities of the objects and altered the contact forces between the robots, as shown in the red areas in Fig. 6 (c) and (d). In terms of position tracking, the difference lies in the fact that the two robot hands followed the object's movements and deviated from the desired paths in the green area in Fig.5 (a). However, under the controller (58), the robots keep the same trajectories, satisfying the position tracking requirements.

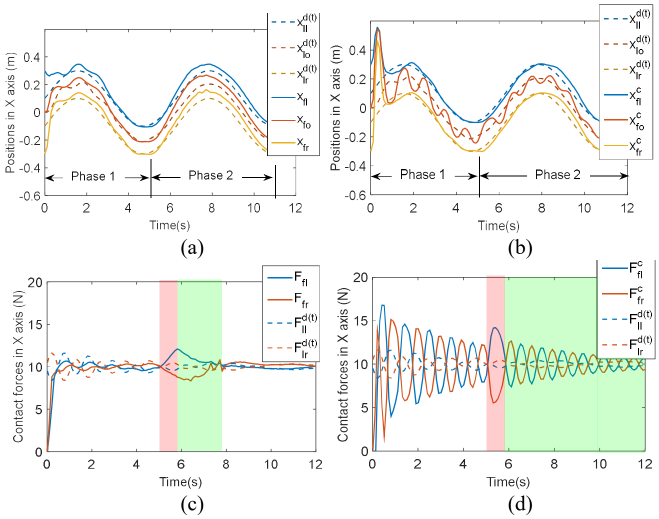

Fig. 7. Trajectories of leaders, followers and object and contact forces of the proposed method ((23) and (34)) and comparative method ((58) and (34)) with external force and $M_o = 3kg$ **(a)** Positions in X axis of the proposed methods; **(b)** Positions in X axis of the comparative methods; **(c)** Contact forces of the proposed methods; **(d)** Contact forces of the comparative methods.

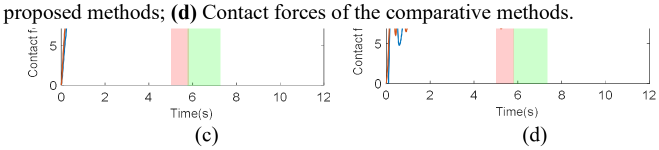

Fig. 6. Trajectories of leaders, followers and object center, and contact forces of the proposed method ((23) and (34)) and comparative method ((58) and (34)) with external force **(a)** Positions in X axis of the proposed methods; **(b)** Positions in X axis of the comparative methods; **(c)** Contact forces of the proposed methods; **(d)** Contact forces of the comparative methods.

The force acting on the object results in minor variations in its position and affects the robot's contact force. To verify this effect, we modified the mass of the object from 1 kg to 3 kg and ran another experiment under the same conditions as shown in Fig. 6. The experimental results are presented in Fig. 7, which divides the process into two phases. During the first phase (0s to 5s), both the positions and contact forces remain stable under the controller (23). However, in the second phase (after 5s), the object oscillates between two robots, resulting in large fluctuating forces under the control of (58). A comparison between the results in the first phase and those in Fig. 5 (a) indicate that the trajectories of the object and robots are altered in both algorithms. In phase 2, the external forces exacerbate the oscillations of the object, making it challenging to stabilize within a short time. Nonetheless, the proposed method manages to stabilize the object within a reasonable timeframe from 7.2s to 7.8s. This implies that the robots first stabilize the object and then meet the self-positioning requirements.

Accurate estimates of object dynamics significantly enhance the tracking performance. Fig. 8 illustrates the values of the object dynamics on the leader and follower sides, as well as the estimations of the following robots. Fig. 8 (a) and (b) show the results for two cases $M_o = 1kg$ and $M_o = 3kg$. The zoomed-in figure in Fig.8(a) reveals that the differences in object dynamics Φ_o between the estimations and real values are negligible. However, some errors are observed during the initial and state-switching phases. Conversely, when using the controller (58) results, much larger but decaying fluctuating errors will occur, which is the primary reason for object position variations and robot force tracking errors.

C. Violation of constraints

The final experiment aims to examine if the performance of the joints can meet the desired specifications, and whether the errors can be kept within predesigned bounds. To achieve this, we conduct the experiment with the condition $M_o = 1kg$. The blue dashed lines shown in Fig. 9 (a) indicate the prescribed boundaries for the joint errors, while the red solid curves represent the bounds after adding Δx, and the orange solid curves represent the joint errors. It can be observed that the joint errors decrease to 0 within the first 2 seconds, and the prescribed upper and lower boundaries remain stable between

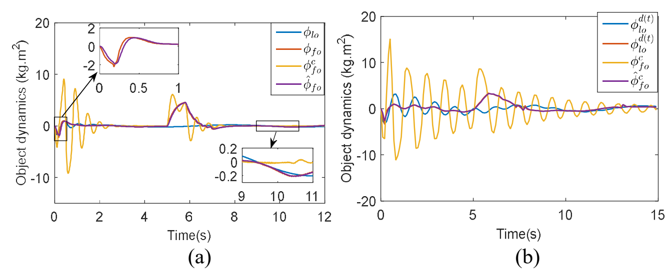

Fig. 8. Compare of the object dynamics **(a)** Results of the case $M_o = 1kg$ **(b)** Results of the case $M_o = 3kg$.

2s to 5s when the object is stably grasped.

After 5s, under the influence of the external force ΔF, the joint errors increase or sometimes even exceed the original limits in Fig. 9 (c). In our previous research, uncertain dynamics terms were estimated and compensated to ensure that the joint errors remained within the prescribed limits. However, there were still some errors and possibilities of breaking the position constraints [31]. The proposed method employs varying bounds based on the impedance model, and the boundary conditions are strictly enforced. This approach provides a more robust and reliable solution for the joint control, reducing the likelihood of constraint violations. Although the experiment is conducted using a dual-arm robot teleoperation system, it can be applied to teleoperation systems consisting of more than two robot arms or robot hand manipulations.

VI. Conclusion

This paper presents a hierarchical control method based on a new force-object dynamics observer and improved BLFs for manipulating deformable objects using a multi-robot teleoperation system. The proposed method effectively estimates the hybrid object dynamics to achieve the desired operational performance and reduce the fluctuations of the object caused by unbalanced contact forces. Even when the object is disturbed by external forces, the proposed scheme can quickly mitigate the influence caused by the disturbance and restore the position tracking and stable contact manipulation as instructed by the operators. The experiments demonstrate that the proposed method can outperform previous pure position tracking methods in terms of stabilizing the status of the object, cooperation among multiple robots, and robustness to unknown disturbances.

However, there are still some challenging issues related to teleoperation for deformable objects and soft tissue that require further investigation, such as the stiffness and viscosity of the object. In the future, it is important to apply the proposed framework to various robotic manipulations, such as object gripping, placing, and ultrasound scanning on phantoms.

References

[1] C. Meeker, M. Haas-Heger and M. Ciocarlie, "A Continuous Teleoperation Subspace With Empirical and Algorithmic Mapping Algorithms for Nonanthropomorphic Hands," *IEEE T. Autom. Sci. Engin.*, vol. 19, no. 1, pp. 373-386.

[2] J. Li, Z. Li, Y. Feng, Y. Liu and G. Shi, "Development of a Human–Robot Hybrid Intelligent System Based on Brain Teleoperation and Deep Learning SLAM," *IEEE T. Autom. Sci. Engin.*, vol. 16, no. 4, pp. 1664-1674, Oct. 2019.

[3] D. Huang, B. Li, Y. Li and C. Yang, "Cooperative Manipulation of Deformable Objects by Single-Leader–Dual-Follower Teleoperation," *IEEE T. Ind. Electron.,* vol. 69, no. 12, pp. 13162-13170, 2022.

[4] D. Huang, C. Yang, M. Li, H. Huang and Y. Li, "Motion Regulation Solutions to Holding & Moving an Object for Single-Leader-Dual-Follower Teleoperation," *IEEE T. Ind. Inform.*, doi: 10.1109/TII.2022. 3229149.

[5] M. Shahbazi, S. F. Atashzar, and R. V. Patel, "A systematic review of multilateral teleoperation systems," *IEEE T. Haptics*, vol. 11, no. 3, pp. 338-356, 2018.

[6] D. Sun, Q. Liao and A. Loutfi, "Single Master Bimanual Teleoperation System With Efficient Regulation," *IEEE T. Robot.*, vol. 36, no. 4, pp. 1022-1037

[7] C. Zhou, L. Zhao, H. Wang, L. Chen and Y. Zheng, "A Bilateral Dual-Arm Teleoperation Robot System with a Unified Control Architecture," in *30th IEEE International Conference on Robot & Human Interactive Communication (RO-MAN)*, Vancouver, BC, Canada, 2021, pp. 495-502,

[8] S. Sirouspour. "Modeling and control of cooperative teleoperation systems," *IEEE T. Robot*., vol. 21, no. 6, pp. 1220-1225, Dec. 2005.

[9] Z. Chen, F. Huang, W. Chen, J. Zhang, W. Sun, J. Chen, J. Gu, and S. Zhu, "RBFNN-based adaptive sliding mode control design for delayed nonlinear multilateral telerobotic system with cooperative manipulation," *IEEE T. Ind. Inform.*, vol. 16, no. 2, pp. 1236-1247, 2019.

[10] Z. Chen, Y. J. Pan, and J. Gu, "Integrated adaptive robust control for multilateral teleoperation systems under arbitrary time delays," *Int. J. Robust Nonlin. Control.*, vol. 26, no. 12, pp. 2708-2728, 2016.

[11] N. T. Thanh, X. Jiang, S. Abiko, T. Tsujita, A. Konno, and M. Uchiyama, "Collaborative haptic interaction in virtual environment of multi-operator multi-robot teleoperation systems." in *2012 Proceedings of SICE Annual Conference (SICE)*, Akita, Japan, 2012 pp. 1585-1590.

[12] F. Azimifar, S. Ahmadkhosravi Rozi, A. Saleh, and I. Afyouni, "Transparency performance improvement for multi-master multi-slave teleoperation systems with external force estimation," *T. I. Meas. Control,* vol. 40, no. 13, pp. 3851-3859, 2018.

[13] D. Sun, Q. Liao, X. Gu, C. Li, and H. Ren, "Multilateral teleoperation with new cooperative structure based on reconfigurable robots and type-2 fuzzy logic," *IEEE T. Cyber.*, vol. 49, no. 8, pp. 2845-2859, 2018.

[14] G. Peng, C. Yang, W. He, and C. P. Chen, "Force sensorless admittance control with neural learning for robots with actuator saturation," *IEEE T. Ind. Electron.*, vol. 67, no. 4, pp. 3138-3148, 2019.

[15] C. Yang, G. Peng, L. Cheng, J. Na, and Z. Li, "Force sensorless admittance control for teleoperation of uncertain robot manipulator using neural networks," *IEEE T. Sys., Man, and Cyber.: Syst.,* Vol.51, No. 5, pp. 3282-3292, 2019.

[16] G. Peng, C. P. Chen, W. He, and C. Yang, "Neural-Learning-Based Force Sensorless Admittance Control for Robots with Input Deadzone," *IEEE T. Ind. Electron*., vol. 68, no. 6, pp. 5184 – 5196, 2020.

[17] A. Flores-Abad, M. Nandayapa, and M. A. Garcia-Teran, "Force sensorless impedance control for a space robot to capture a satellite for on-orbit servicing." in *2018 IEEE Aerospace Conference. IEEE*, : Big Sky, MT, USA, 2018, pp.1-7.

[18] C. Passenberg, A. Peer and M. Buss, "Model-Mediated Teleoperation for multi-operator multi-robot systems," in *2010 IEEE/RSJ International Conference on Intelligent Robots and Systems*, 2010, pp. 4263-4268,

[19] V. E. Arriola Rios. "Learning to predict the behaviour of deformable objects through and for robotic interaction." *PhD diss., University of Birmingham*, 2013.

[20] Z. Lu, P. F. Huang, and Z. X. Liu, "Predictive approach for sensor-less bimanual teleoperation under random time delays with adaptive fuzzy control", *IEEE T. Ind. Electron.*, vol. 65, no. 3, pp. 2439–2448, Mar. 2018.

[21] Z. Lu, P. Huang, and Z. Liu, "High-gain nonlinear observer-based impedance control for deformable object cooperative teleoperation with nonlinear contact model," *Int. J. Robust Nonlin. Control,* vol. 30, no. 4, pp. 1329-1350, 2020.

[22] Z. Lu, P. Huang, and Z. Liu, "Relative impedance-based internal force control for bimanual robot teleoperation with varying time delay," *IEEE T. Ind. Electron.*, vol. 67, no. 1, pp. 778-789, 2019.

[23] Z. Lu, P. Huang, Z. Liu, and H. Chen, "Fuzzy-observer-based hybrid force/position control design for a multiple-sampling-rate bimanual teleoperation system," *IEEE T. Fuzzy Syst.*, vol. 27, no. 7, pp. 1383-1396, 2018.

[24] C. Yang, Y. Jiang, Z. Li, W. He, and C.-Y. Su, "Neural control of bimanual robots with guaranteed global stability and motion precision," *IEEE T. Ind. Inform.*, vol. 13, no. 3, pp. 1162-1171, 2016.

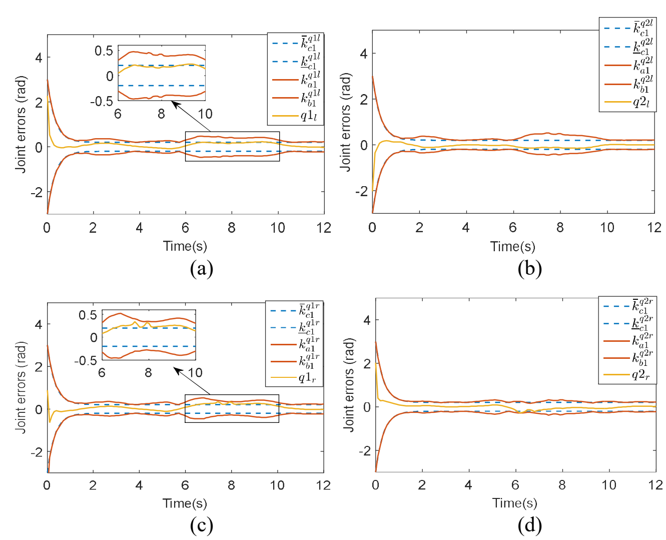

Fig. 9. Joint tracking errors with varying boundaries. **(a)** Results of joint 1 of the left robot arm **(b)** Results of joint 2 of the left robot arm **(c)** Results of joint 1 of the right robot arm **(d)** Results of joint 2 of the right robot arm.

[25] D. Huang, H. Zhan, and C. Yang, "Impedance Model-Based Optimal Regulation on Force and Position of Bimanual Robots to Hold an Object," *Complexity*, vol. 2020, 2020.
[26] W. He, Y. Sun, Z. Yan, C. Yang, Z. Li, and O. Kaynak, "Disturbance observer-based neural network control of cooperative multiple manipulators with input saturation," *IEEE T. Neur. Net. Lear. Syst.*, vol. 31, no. 5, pp. 1735-1746, 2019.
[27] V. R. Garate, S. Gholami and A. Ajoudani, "A Scalable Framework for Multi-Robot Tele-Impedance Control," *IEEE T. Robot.*, vol. 37, no. 6, pp. 2052-2066, Dec. 2021.
[28] D. Lee, and M. W. Spong. "Bilateral teleoperation of multiple cooperative robots over delayed communication networks: Theory," in *IEEE ICRA*, Orlando, Florida, USA, 2006, pp. 360-365.
[29] D. Lee, A. Franchi, H. Son, C. S. Ha, H. H. Bülthoff, and P. R. Giordano. "Semiautonomous haptic teleoperation control architecture of multiple unmanned aerial vehicles," *IEEE/ASME T. Mech.*, vol. 18, no. 4, pp. 1334-1345, Aug. 2013.
[30] D. Lee, "Passive decomposition and control of nonholonomic mechanical systems," *IEEE T. Robot.*, vol. 26, no. 6, pp. 978-992, Feb. 2010.
[31] C. Yang, Y. Jiang, Z. Li , W. He, and C. Y. Su, "Neural control of bimanual robots with guaranteed global stability and motion precision." *IEEE T. Ind. Inform.*, vol. 13, no. 3, pp. 1162-1171, 2016.
[32] J.-J. Slotine, "Robustness issues in robot control," *in Proc. IEEE Int. Conf. Robot. Autom.* , Mar. 1985, vol. 2, pp. 656–661.
[33] Y. J. Liu and S. Tong, "Barrier Lyapunov functions-based adaptive control for a class of nonlinear pure-feedback systems with full state constraints," *Automatica*, vol. 64, pp. 70–75, Feb. 2016
[34] Z. Ma, and P. Huang, "Adaptive Neural-Network Controller for an Uncertain Rigid Manipulator With Input Saturation and Full-Order State Constraint," *IEEE T. on Cyber.*, 2020. In press.
[35] A. Gil, O. Reinoso, J. M. Marin, L. Paya, and J. Ruiz, "Development and deployment of a new robotics toolbox for education." *Comput. Appl. Eng. Educ.*, vo.23, no.3, pp.443-454, 2015.

Zhenyu Lu (M'21) He is currently working as a senior research fellow in Bristol Robotic Laboratory & University of the West of England, Bristol. He received the Ph.D. degree in Northwestern Polytechnical University, Xi'an, China in 2019. His research interests include teleoperation, human–robot interaction and intelligent learning method.

Ning Wang (S'07-M'11) is a Senior Lecturer in Robotics at the Bristol Robotics Laboratory, University of the West of England, United Kingdom. She received the M.Phil. and Ph.D. degrees in electronics engineering from the Department of Electronics Engineering, The Chinese University of Hong Kong, Hong Kong, in 2007 and 2011, respectively. Her research interests lie in signal processing, intelligent data analysis, human-robot interaction and autonomous driving.

Weiyong Si received the M.S. degree from the Beijing Institute of Technology in 2018. He is currently pursuing the PhD degree in Bristol Robotics Laboratory and the University of the West of England. His research interests include robot skill learning, teleoperation, and robot control.

Chenguang Yang (M'10-SM'16) received the Ph.D. degree in control engineering from the National University of Singapore, Singapore, in 2010, and postdoctoral training in human robotics from the Imperial College London, London, U.K. He was awarded UK EPSRC UKRI Innovation Fellowship and individual EU Marie Curie International Incoming Fellowship. As the lead author, he won the IEEE Transactions on Robotics Best Paper Award (2012) and IEEE Transactions on Neural Networks and Learning Systems Outstanding Paper Award (2022). He is the Corresponding Co-Chair of IEEE Technical Committee on Collaborative Automation for Flexible Manufacturing, a Fellow of Institute of Engineering and Technology (IET), and a Fellow of British Computer Society (BCS). His research interest lies in human robot interaction and intelligent system design.